UDC 551.558.29:551.515.11:551.511.2(263.5) "1965.10"

VERTICAL MOTIONS AND THE KINETIC ENERGY BALANCE OF A COLD LOW

BANNER I. MILLER and TOBY N. CARLSON
National Hurricane Research Laboratory, ESSA, Miami, Fla.

ABSTRACT

Vertical motions have been computed for a 6-day period during which an upper tropospheric cold Low moved through the eastern Caribbean, and a kinetic energy budget for the region has been constructed. During the first 3 days, the kinetic energy inside the volume increased. The computations indicate that the increase was caused by lateral advection of kinetic energy into the volume plus a small internal conversion of potential to kinetic energy. The kinetic energy decreased during the last 3 days, as the circulation became indirect. Visual agreement between the vertical motions and the observed weather was good.

1. INTRODUCTION

Analyses of the data from Project ECCRO (Carlson 1967*a*, 1967*b*) have provided one of the most complete descriptions in existence of an upper tropospheric cold Low. Data were collected by research aircraft at five levels, ranging from 976 to 238 mb, and extended over a 6-day period in October 1965. While the analyses cover only a limited geographical area (fig. 1), the data offer a unique opportunity for studying the structure and energetic processes of a cold Low, a common feature of the lower latitudes in summer (Ricks 1959, Frank 1966). The data also appear to be of sufficient accuracy to permit meaningful testing of some of the features of dynamical models. This paper will present selected vertical motion patterns along with some of the energy transformations associated with the passage of a cold Low over the network of stations, and make an attempt to assess the realism of a numerical model that has been designed for analysis and prediction of tropical weather systems (Miller 1969).

2. MODIFICATION OF THE INITIAL ANALYSES

Carlson (1967*a*, 1967*b*) analyzed the aircraft data, supplemented by conventional upper air soundings from the Caribbean stations, at 976, 841, 692, 501, and 238 mb. The first paper (Carlson 1967*a*) contains a detailed description of Project ECCRO, including a summary of data and selected analyses of the data fields. In the second paper (Carlson 1967*b*), the cold Low was the subject of investigation in which the winds, temperatures, geopotential heights of constant pressure surfaces, and mixing ratios were composited from the individual analyses by means of a sliding average made according to the mean (westward) speed of the cold Low. In this way, an artificially enlarged area was formed that encompassed more of the cold Low than any of the individual analyses. Thus, the original 10×13 grid was expanded in the composite to a 10×19 grid, the spacing being 1° of longitude for both grids (108 km).

Calculations of vertical motion were performed for a seven-level model (Miller 1969), the levels ranging from 1000 to 100 mb, with a pressure increment of 150 mb. The u and v components of the wind field at 100 mb were obtained from the stream function, which was obtained from the analyzed height field by solving the balance equation. At both 250 and 100 mb, the mixing ratio was obtained by assuming a constant value of 50 percent relative humidity, since mixing ratios were not measured above 500 mb. This is not critical since the variation of moisture at these levels (and low temperatures) is not of great significance in the model. Values of u, v, and q were obtained at 550 and 400 mb by linear interpolation from the levels used on Carlson's analyses. Geopotential heights for these levels were obtained by logarithmic variation between existing analyses. Carlson's analyses for the 976-, 841-, 691-, and 238-mb levels were accepted for the 1000-, 850-, 700-, and 250-mb levels.

It was felt that the small grid area and relatively large number of boundary grid points (approximately one-third of the total grid points) would have a deleterious effect on the results calculated within the boundaries. By quadratic interpolation between the original grid points, a number of additional points were generated to somewhat reduce the boundary effects. The individual 10×13 array was thus expanded to a 19×23 array (51-km spacing at 22.5° N.), and the composite grid expanded to 15×19 points (grid length 66 km at 22.5° N.).

Carlson's examination of the original fields, from a purely kinematic standpoint, revealed that the basic wind fields contained small-scale spurious fluctuations which were the result of inconsistencies in the basic raw data. For minimizing this, the u and v components of the wind were smoothed once in the horizontal, using a nine-point operator and a smoothing coefficient of 0.50. The fields were also smoothed in the vertical, using a three-point centered smoothing in which one-quarter of the values on the adjacent levels above and below were

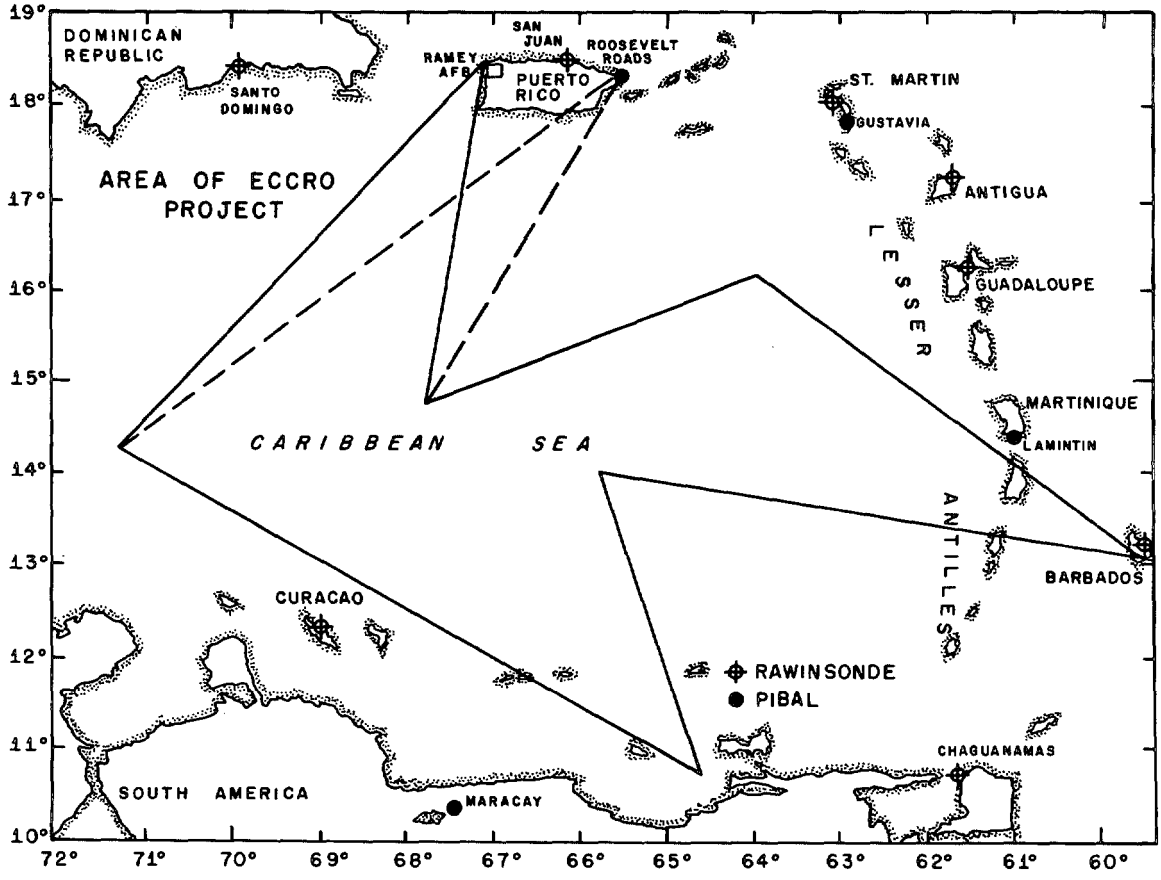

FIGURE 1.—Map showing area of Project ECCRO. The flight path is shown by the connected line segments (shown dashed for track of Navy aircraft).

added to half the central value. Vertical smoothing was not done at 400 and 250 mb to avoid smoothing the actual vertical wind shears which varied rapidly with height at these levels. Smoothing these fields was found to reduce the implicit temperature gradients in the upper troposphere in an unacceptable manner.

Carlson attempted a rough hydrostatic balance between his temperature and height analyses. However, some degree of independency remained in the height, temperature, and wind fields. To obtain a set of data as internally consistent as possible, we used the following procedure, referred to as method A:

1) The smoothed winds were accepted as the most reliable data for the daily calculations. On the 13th and 17th, the time-dependent terms in the divergence and omega equations were evaluated by taking the averages of the observed changes over 2-day periods (12–14 and 16–18).

2) The height of the northwestern grid point was accepted as analyzed. Other boundary heights were generated from the normal wind component, assuming geostrophic balance, and applying a small correction to insure that the height returned to its initial value at the starting point following the taking of the line integral.

3) A first estimate of the height field was obtained by solving the divergence equation

$$\frac{\partial D}{\partial t}+\mathbf{V}\nabla D+\omega\frac{\partial D}{\partial p}+D^2-2J(u,v)-f\zeta+\beta u \times\frac{\partial\omega}{\partial x}\frac{\partial u}{\partial p}+\frac{\partial\omega}{\partial y}\frac{\partial v}{\partial p}-K_h\nabla^2 D-g\frac{\partial}{\partial p}\left(\frac{\partial\tau_x}{\partial x}+\frac{\partial\tau_y}{\partial y}\right)+\nabla^2\phi=0. \quad (1)$$

(See the list of symbols at the end of this section.) At this point, both the divergence and the vertical motion were set equal to zero; this procedure is approximately equivalent to solving the balance equation with friction.

4) The temperatures were computed from the geopotential field obtained from equation (1); the lapse rate for the lower layer was specified.

5) The vertical motion was obtained by solving the omega equation (5) in section 3. Time-dependent terms were evaluated.

6) A new wind field was constructed by adding the divergent and rotational components obtained after solving

$$\nabla^2\psi=\frac{\partial v}{\partial x}-\frac{\partial u}{\partial y} \quad (2)$$

and

$$\nabla\chi=-\frac{\partial\omega}{\partial p}. \tag{3}$$

Boundary values for ψ were determined from the tangential component of the wind (Sanders and Burpee 1968); χ was set equal to zero on the boundary.

7) The divergence was computed from the omega field, and a second estimate of the heights was obtained by solving equation (1) again. The time-dependent term in equation (1) was a 48-hr average of $\partial D/\partial t$, the divergences at $t-24$ and $t+24$ hr being obtained from preliminary estimates of omega obtained in a manner to be described later. Temperatures were recomputed.

For the composited data, the wind field obtained from the analyzed heights via the balance equation

$$f\nabla^2\psi+\beta\frac{\partial\psi}{\partial y}+2\left(\frac{\partial^2\psi}{\partial x^2}\frac{\partial^2\psi}{\partial y^2}-\left(\frac{\partial^2\psi}{\partial y\partial x}\right)^2\right)=\nabla^2\phi \tag{4}$$

resulted in vertical motions that appeared to fit the weather patterns better than those generated by the procedure described above. The difference in results may be attributable to the difference in the way the scalar height and vector wind fields were composited, or to a greater amount of noise in the composited wind field. In the composite case, all time-dependent terms were set equal to zero, since they could not be realistically evaluated, and since it was reasoned that the compositing procedure resulted in a relatively steady state, although a somewhat fictitious description of the cold Low.

Symbols in this report have the following meanings:

c_d	drag coefficient,
c_p	specific heat of air at constant pressure,
D	divergence,
f	Coriolis parameter,
f_0	mean value of Coriolis parameter,
F_q	flux of water vapor,
F_s	flux of sensible heat,
g	acceleration of gravity,
H	total heating function,
H_s	sensible heat (cal gm^{-1} sec^{-1}),
H_1	latent heat (cal gm^{-1} sec^{-1}),
I	net moisture convergence,
J	Jacobian operator,
K	kinetic energy per unit mass,
K_h	a coefficient for lateral mixing,
K_m	a coefficient for vertical mixing,
L	latent heat of condensation,
m	map scale factor,
p	pressure,
q	mixing ratio,
q_s	saturated mixing ratio,
Q	total moisture required to saturate and warm a column,
R	gas constant,
s	distance,
t	time,
T	temperature,
T^*	virtual temperature,
u	zonal component of the wind,
v	meridional component of the wind,
V_0	wind speed at the surface,
v_r	radial wind speed,
$\mathbf{V}$	horizontal velocity vector,
x	distance in east-west direction,
y	distance in north-south direction,
α	specific volume,
β	df/dy
ζ	relative vorticity,
η	absolute vorticity,
θ	potential temperature,
π	RT/pT,
ρ	density,
σ	static stability $-\alpha\partial\theta/\theta\partial p$,
τ_x,τ_y	horizontal shearing stresses,
ϕ	geopotential,
χ	velocity potential,
ψ	stream function,
ω	dp/dt, vertical p velocity, and
∇^2	horizontal Laplacian operator.

3. SOLUTION OF THE OMEGA EQUATION

The vertical motions were obtained by solving a diabatic and viscous omega equation

$$\nabla^2\sigma\omega+f_0\eta\frac{\partial^2\omega}{\partial p^2}-f_0\omega\frac{\partial^2\eta}{\partial p^2}-f_0\frac{\partial}{\partial p}\left(\frac{\partial\omega}{\partial x}\frac{\partial v}{\partial p}-\frac{\partial\omega}{\partial y}\frac{\partial u}{\partial p}\right)$$
$$=f_0\frac{\partial}{\partial p}(\mathbf{V}\cdot\nabla\eta)-f_0K_H\nabla^2\frac{\partial\eta}{\partial p}-f_0g\frac{\partial^2}{\partial p^2}\left(\frac{\partial\tau_y}{\partial x}-\frac{\partial\tau_x}{\partial y}\right)$$
$$+\pi\nabla^2(\mathbf{V}\cdot\nabla\theta)-\nabla^2\left[\frac{R}{p}\frac{\partial}{\partial p}\left(\rho^2g^2K_m\frac{\partial\theta}{\partial p}\right)\right]$$
$$-\nabla^2\frac{R}{p}(K_H\nabla^2\theta)-\nabla^2\frac{R}{p}\frac{H}{c_p}+\pi\nabla^2\frac{\partial\theta}{\partial t}+f\frac{\partial}{\partial t}\left(\frac{\partial\eta}{\partial p}\right). \tag{5}$$

Equation (5), described by Miller (1969), will not be discussed in detail here, but we will, however, summarize the manner in which the diabatic effects were evaluated.

The total heat source, H, may be expressed as the sum of the latent heat, H_l, and the sensible heat, H_s, added to system. The fluxes of water vapor and sensible heat at the surface are proportional to the surface wind, the drag coefficient, and the air-sea differences in temperature and mixing ratio:

$$F_s=\rho_0c_dc_p(T_w-T_a)V_0 \tag{6a}$$

and

$$F_q=\rho_0c_d(q_w-q_a)V_0. \tag{6b}$$

Here, the subscripts w and a refer to values taken at the sea surface and at the lowest level of analyses, respectively. The air-sea temperature difference was assumed to be

2° and ($q_w - q_a$) was held fixed on the assumption of a 3° difference in dew point and temperature from the sea surface to the lowest level. These quantities F_s and F_q were assumed to decrease linearly with pressure and were allowed to go to zero at 700 mb, that is, $H_s = g(\partial F_s/\partial p)$. This technique is consistent with the maintenance of a quasi-moist adiabatic lapse in the lowest layers and permits the upward transport of sensible heat against a potential temperature gradient. Over water, the drag coefficient was made an empirical function of the wind speed, and over land a constant value of 0.005 was assumed. Sensible heat and evaporation were set equal to zero over land.

The latent heat added to the system was composed of two parts, first being a parameterization of the heat released by cumulus convection, HL_1, originally proposed by Kuo (1965). Kuo defined a quantity, Q, as the moisture required to saturate the atmosphere and (following condensation of a portion of the water vapor) to raise its temperature to that of the moist adiabat passing through the base of the cloud. Q is defined as

$$Q = \int_{p_b}^{p_t} (q_s - q) \frac{\delta p}{g} + \int_{p_b}^{p_t} \frac{c_p}{L} (T_s - T) \frac{\delta p}{g}. \tag{7}$$

The net moisture convergence within a column may be obtained by

$$I = -\int_{p_b}^{p_t} \frac{\partial q}{\partial t} \frac{\delta p}{g} - \frac{\omega_0 q_0}{g} \tag{8}$$

where q_0 and ω_0 are the mixing ratio and the vertical motion at 1000 mb, p_b and p_t are the pressures at the base and the top of the clouds, q_s and T_s refer to the saturation mixing ratio and temperature along the moist adiabat determined by the lifting condensation level of the sub-cloud air, while T and q refer to the environmental conditions. Forty-eight-hour averages computed from known values were used for $\partial q/\partial t$. The heating function may now be expressed by

$$HL_1 = \frac{I}{Q} c_p (T_s - T). \tag{9}$$

HL_1 is set equal to zero at 1000 and 100 mb, if I is zero or negative, or if T is equal to or greater than T_s. It will be noted that the Kuo heating function is self-limiting, since it tends to approach zero as the lapse rate within the cloud becomes moist adiabatic and the cloud becomes saturated.

The second part of the latent heat release is due to the ascent of moist air with the broad-scale vertical motion. It was defined as

$$HL_2 = -c_p \left[\frac{L}{c_p} \frac{\partial q_s}{\partial p}\right] \omega. \tag{10}$$

An examination of the variation of the saturation mixing ratio with pressure shows that the variation is almost linear for the tropical atmosphere within the range from 700 to 200 mb. Accordingly, the quantity in the brackets was set equal to a constant and has the value of 0.06; this was done to speed up the calculations. (The total heating function H is the sum of $HL_1 + HL_2 + H_s$.)

TABLE 1.—*Correlation coefficients and standard deviations of vertical motions computed by methods* A *and* B

Level (mb)	r (13)	σA (13)	σB (13)
1000	0.9996	0.4527×10^{-3}	0.4533×10^{-3}
850	.9651	$.8788\times10^{-4}$	$.8942\times10^{-4}$
700	.9899	$.1249\times10^{-3}$	$.1298\times10^{-3}$
550	.9909	$.7853\times10^{-4}$	$.8179\times10^{-4}$
400	.9890	$.1389\times10^{-3}$	$.1308\times10^{-3}$
250	.9947	$.3755\times10^{-4}$	$.3491\times10^{-4}$
	r (17)	σA (17)	σB (17)
1000	0.9980	0.3445×10^{-3}	0.3758×10^{-3}
850	.9826	$.1255\times10^{-3}$	$.1371\times10^{-3}$
700	.9733	$.5647\times10^{-4}$	$.6516\times10^{-4}$
550	.9919	$.1034\times10^{-3}$	$.1213\times10^{-3}$
400	.9926	$.1428\times10^{-3}$	$.1571\times10^{-3}$
250	.9866	$.3458\times10^{-4}$	$.3882\times10^{-4}$

The omega equation (5) was then solved, subject to the boundary conditions that omega was zero at 100 mb, and that omega at 1000 mb was as proposed by Cressman (1963),

$$\omega_s = \frac{\rho g}{f}\left[\frac{\partial}{\partial y} c_d u V_0 - \frac{\partial}{\partial x} c_d V V_0\right]. \tag{11}$$

4. ALTERNATE METHOD FOR COMPUTING VERTICAL MOTIONS

Since time-dependent terms could be evaluated from known values on only 2 of the 6 days for which data were available, another and somewhat less satisfactory method was used to compute geopotentials, temperatures, and vertical motions. This scheme (referred to as method B) consisted of the following steps:

1) The heights were computed from equation (1) with divergence, omega, and the local time-derivative set equal to zero. The temperatures were computed from the heights and the mixing ratios. These temperatures and heights were accepted as the best obtainable estimates and were used in subsequent calculations.

2) The stream function was obtained from equation (2), and the observed wind was replaced by the rotational wind, which was used in the omega equation.

3) The omega equation was solved with the time-dependent terms assumed to be zero. The sum of these terms is identically zero for a quasi-geostrophic omega equation. The convergence of water vapor, needed to determine the heating function in equation (8) was obtained from the forecast equation,

$$\frac{\partial q}{\partial t} = -u\frac{\partial q}{\partial x} - v\frac{\partial q}{\partial y} - \omega\frac{\partial q}{\partial p} + g\frac{\partial Fq}{\partial p} + K_h\nabla^2 q. \tag{12}$$

Initially, these tendencies were large and seemed to re-

sult in an overestimate of the upward motion in regions of intense convection, as will be seen later. Recalculation of the omegas with $\partial q/\partial t=0$ appeared to give more realistic results.

4) The divergence was computed from the vertical motions, the divergent part of the wind was obtained from the velocity potential derived from equation (3), and the divergent wind was added back to the rotational wind.

Comparisons between vertical motions computed on 2 days by methods A and B are shown in table 1. Differences appear to be small, and the correlation coefficients high. We will, therefore, use the complete set of vertical motions for discussion and energy computations.

5. CORRELATION BETWEEN VERTICAL MOTION AND OBSERVED WEATHER

Selected analyses of the observed wind fields, in the form of analyzed streamlines and isotachs, the vertical motion patterns, the observed distribution of cloud and weather, and the generated (from equation (1)) height and temperature fields are shown in figures 2 through 7, respectively, for the 700- and 250-mb levels on the 13th and 17th of October 1965, and (below) for the composite case. The cold Low was moving westward at a speed of about 6 kt from a position centered just east of the Antilles on the 13th to the vicinity of the Virgin Islands on the 17th. Accompanying the disturbance was an extensive cloud cover situated along its eastern side. Within this cloud shield was a small region of deep cumulonimbus convection southeast of the low center (see fig. 6).

The numerous categories of cloud and weather patterns in figure 6 are presented in an attempt to represent existing conditions in the form of a detailed whole sky code. Basically, the symbols B and C refer to normal or suppressed trade-wind cloudiness; D and E to active to weakly disturbed trade-wind regimes; and I, G, and H to disturbed conditions. The latter three (contained by the scalloped border on the 13th and composite maps) consist of a convective regime I and a nonconvective regime with dense middle and high cloud cover (areas G and H). The symbols X and Y refer to the existence of cirrus layers without a middle cloud cover.

Agreement between cloud cover and vertical motion (figs. 4 and 5) appeared to be the most satisfactory at upper levels in the composite case and least satisfactory at low levels and on the 13th. Strong upward motion (1 to 2 cm sec^{-1}) was occurring over most of the cloud shield on the 17th and in the composite while descending motion or very weak ascent was coinciding with the suppressed areas to the west. On the 13th, the vertical motions show some correspondence between regions of descent and sup-

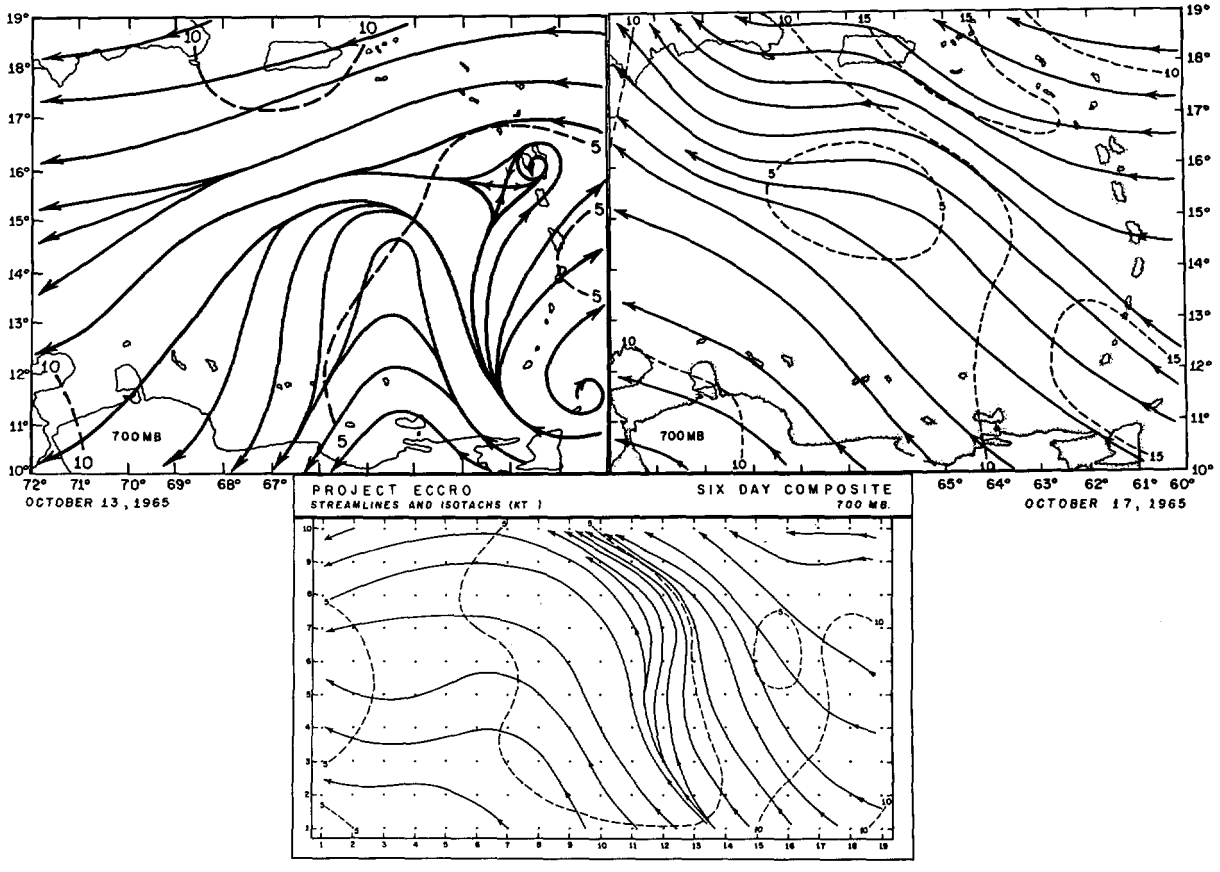

FIGURE 2.—Observed streamline and isotach analyses for the 700-mb level on October 13 (upper left), October 17 (upper right), and for the composited data (below).

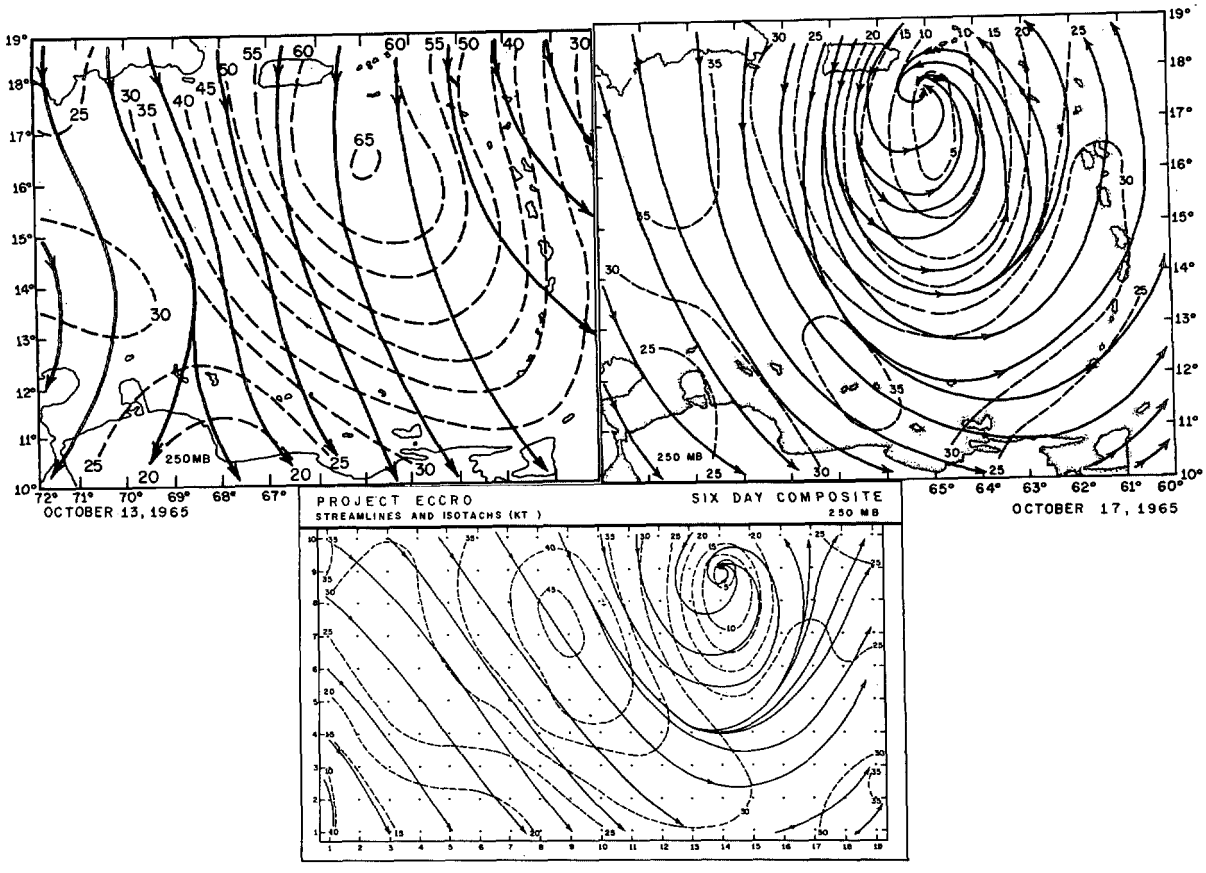

FIGURE 3.—Same as figure 2, but for the 250-mb level.

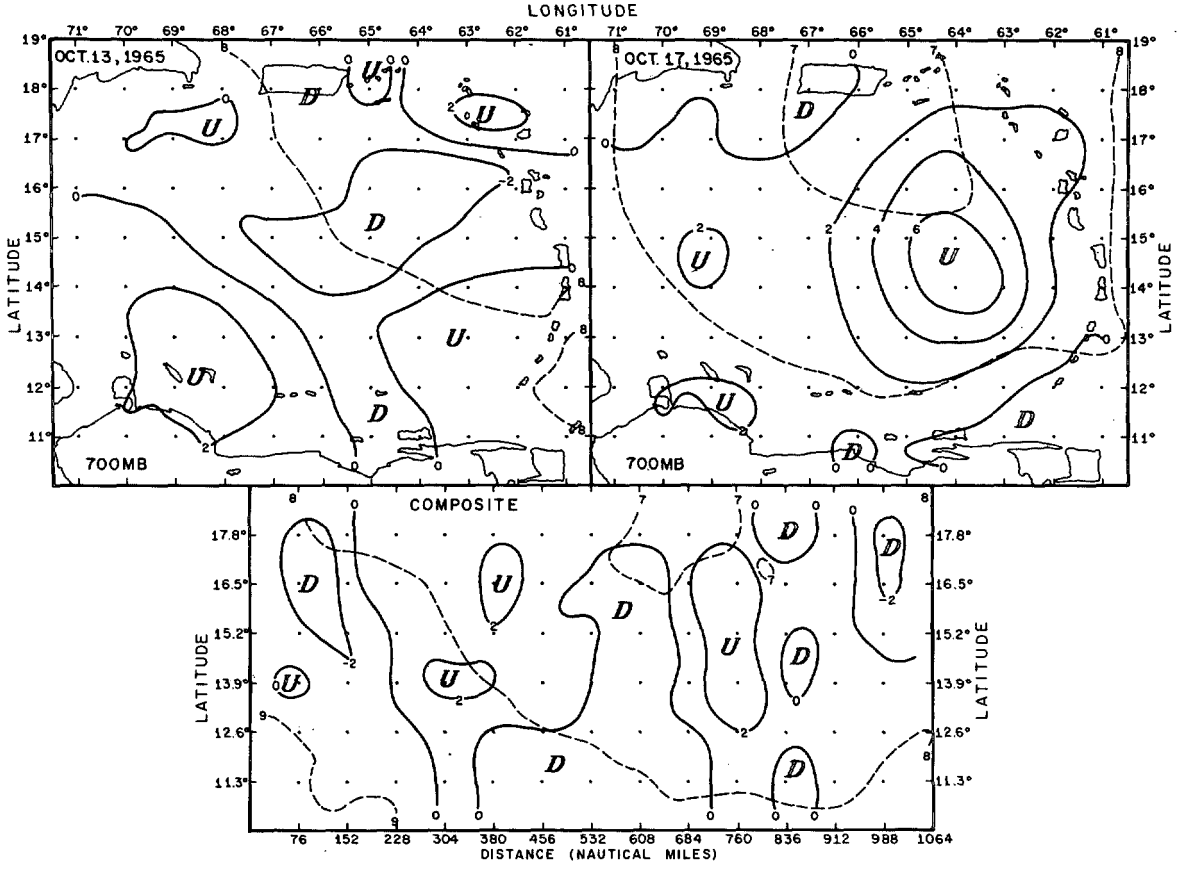

FIGURE 4.—Vertical motions (mm sec^{-1}) and isotherms (°C, obtained from the divergence equation) for the 700-mb level on October 13 (upper left), October 17 (upper right), and for the composited data (below): method B.

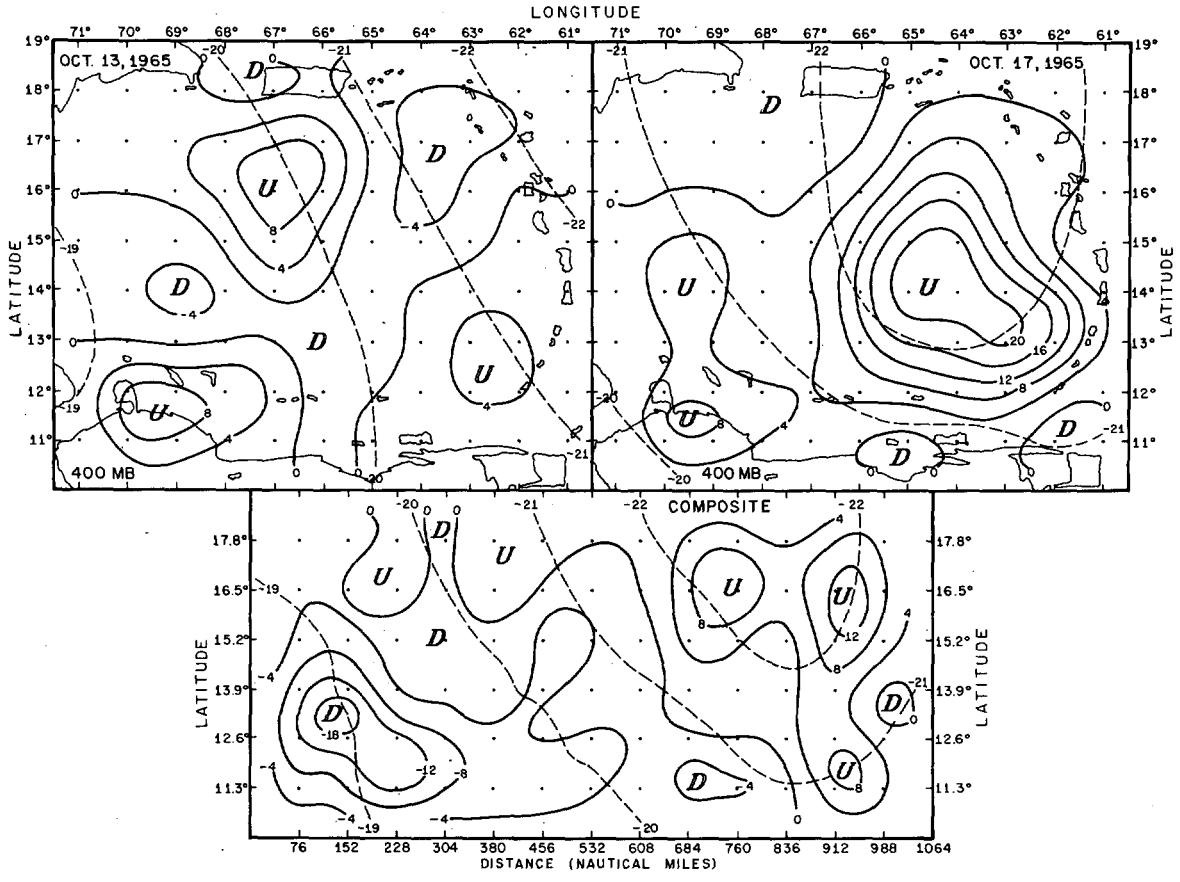

FIGURE 5.—Same as figure 4, but for the 400-mb level.

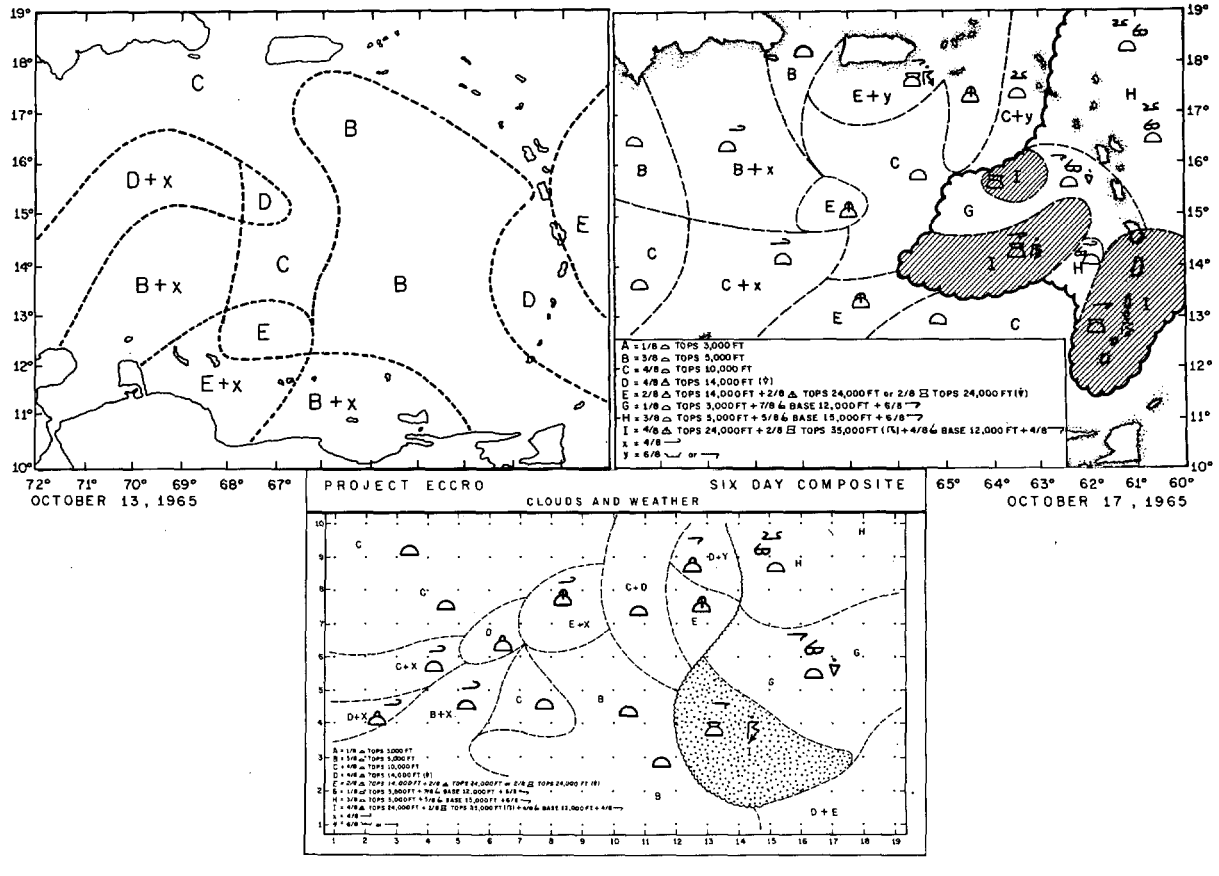

FIGURE 6.—Cloud and weather analysis in the form of whole sky code (see legend) for October 13 (upper left), October 17 (upper right) and composite case (below). The main cloud shield is outlined by a scalloped border. Shading signifies areas in extract deep convection as occurring. Standard meteorological symbols are used.

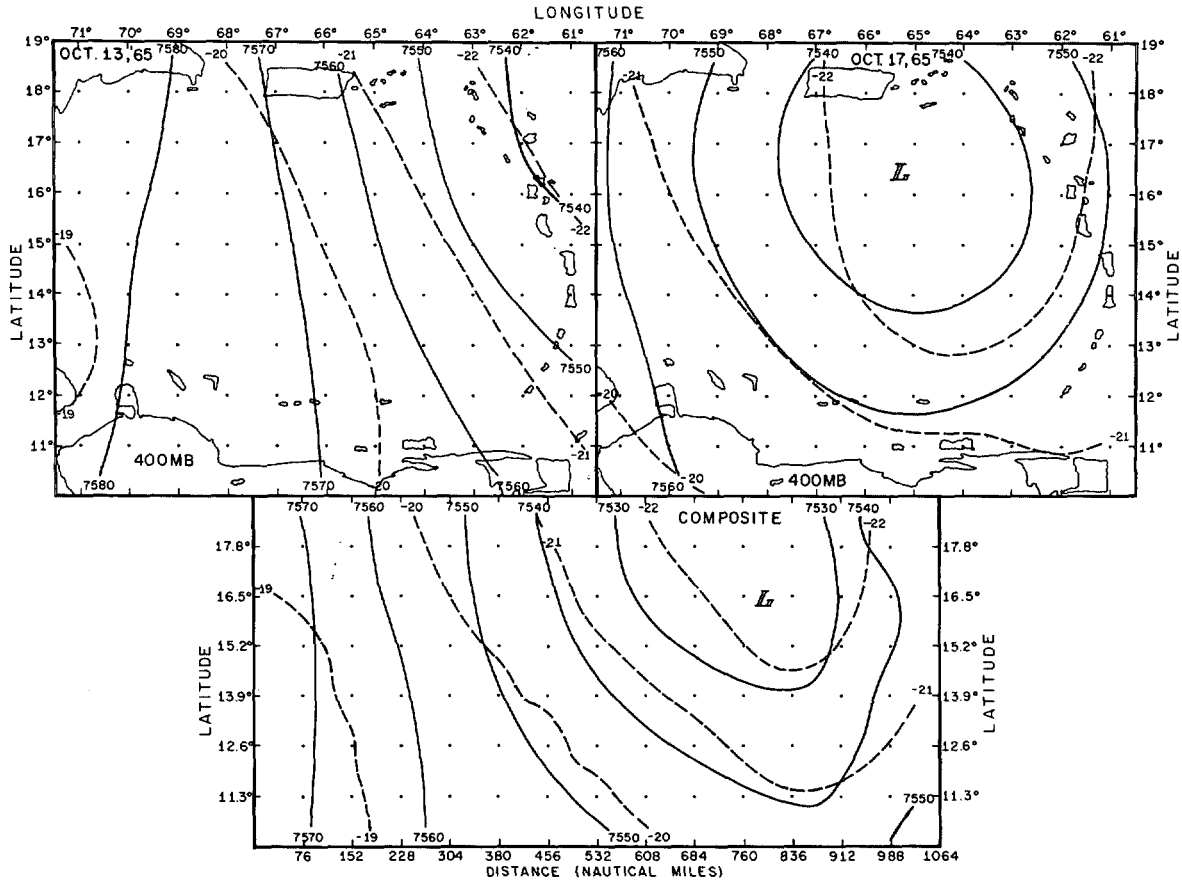

FIGURE 7.—Geopotential contours (meters) and isotherms at 400-mb as derived from the divergence equation for October 13 (upper left), October 17 (upper right), and the composite case (below).

pressed cloudiness, but the ascent is clearly too widespread and intense for the rather inactive conditions which existed on that day (except over South America where cumulus convection was always very active).

The results for the composite case offer the best agreement of all between weather and vertical motion. This outcome may reflect the computational hazards involved in the use of a very small area and a fine grid in synoptic scale work. The pattern of composite vertical motions does not appear to differ very drastically from that presented by Carlson (1967*b*) which was based on a much cruder (kinematic and adiabatic) model. In figures 4 and 5, the composite vertical motions show an essentially cellular pattern at lower levels, with some descending motion in the disturbed region and an area of weak ascent to the west (except in the most suppressed area B where descent predominated). At higher (and strongly baroclinic) levels, the vertical motion pattern supports Carlson's conclusion that the cold Low possesses a dipole pattern of ascent and descent with rising motion (and cloudiness) to the east of the low center and descent dominating on the west. Centers of rising and sinking motion are thus located some distance from the low center, with little significant vertical motion in the center itself.

Additional vertical motion computations (fig. 8) were carried out for the 13th and 17th where in one instance the moisture tendency was not evaluated in the formulation of $H(\partial q/\partial t)=0$ in equation (8) and in the other total heating function was neglected. Neglect of $\partial q/\partial t$ resulted in a visible improvement in the vertical motion calculations. On both the 13th and 17th, most of the ascending motion found in the largely undisturbed areas (B, C, and D) was replaced by weak descent. Within the main cloud shield on the 17th, strength of the ascending motion was reduced by about one-half. Elimination of the heating function itself led to a further reduction in the strength of the updrafts in the disturbed area and over South America, but with little change in the overall pattern. While it may be useful to evaluate the moisture tendency in the heating term in a forecast model such as that described by Miller (1969), the initial tendency appears to affect the computed vertical motions adversely in a nonforecast problem.

Some additional vertical motions, computed by method A, are shown in figure 9. It should also be noted that these resemble more closely those of figure 8 than those of figure 5.

6. THE KINETIC ENERGY BUDGET

The kinetic energy equation may be formed by taking the scalar product of **V** and the vector equation of motion. When integrated over a volume bounded by a lateral boundary L, and having an area A on fixed pressure surfaces in the atmosphere, one obtains (Palmén 1959, Palmén and Holopainen 1962)

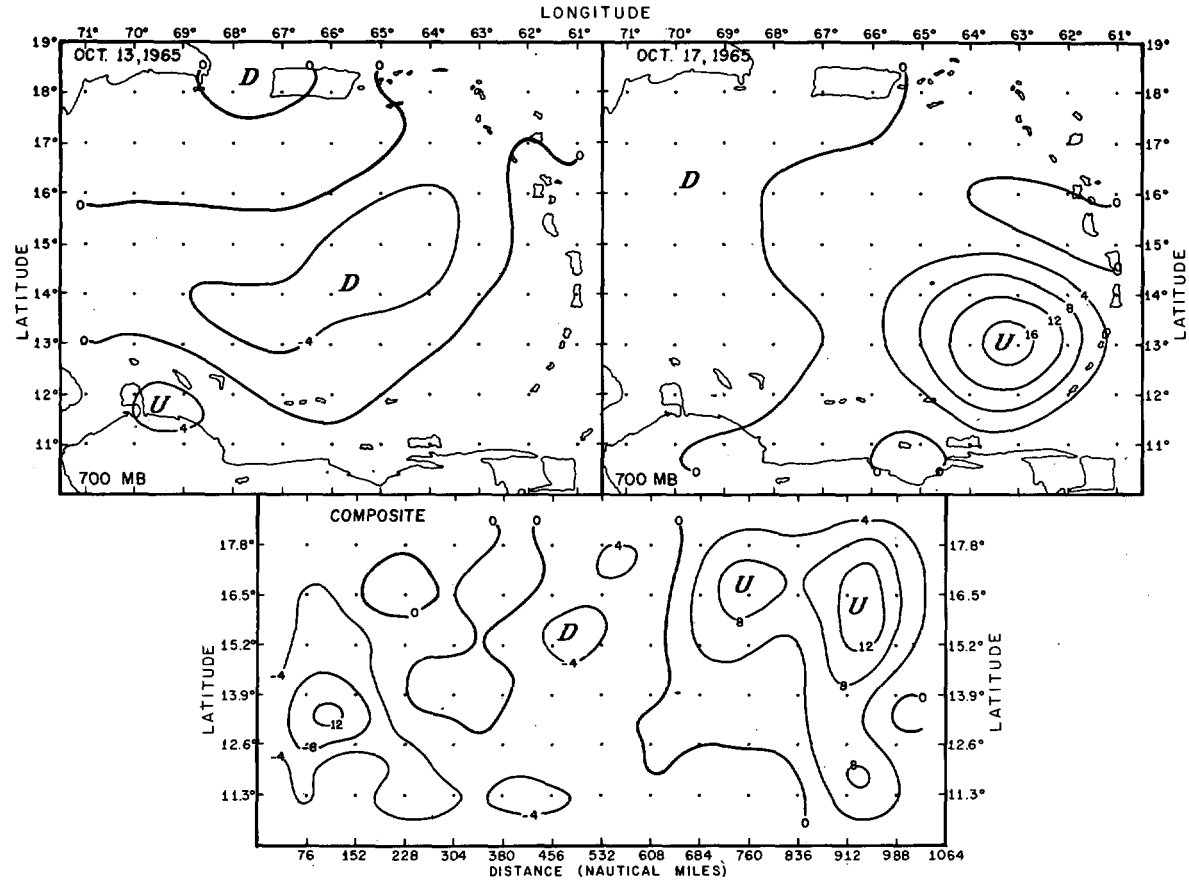

FIGURE 8.—Vertical motions (mm sec^{-1}) computed by evaluation of 3.4 with $I=-\omega_0 q_0/g$.

$$\frac{A}{g}\frac{\partial}{\partial t}\int_{p_h}^{p_0} K dp=-\frac{L}{g}\int_{p_h}^{p_0} KV_h dp+\frac{A}{g}\left[K\omega\right]_{p_h}-\underbrace{\frac{A}{g}\int_{p_h}^{p_0}\mathbf{V}\cdot\nabla\phi dp}_{\text{(term V)}}$$

$$+A\int_0^h\left(u\frac{\partial\tau_{xy}}{\partial z}+v\frac{\partial\tau_{yz}}{\partial z}\right)dz \quad (13)$$

where the first integral on the right is the advection of kinetic energy into the volume through the lateral boundary, the second term is the export of kinetic energy through the top pressure surface, the third integral (term V in table 2) is the production of kinetic energy by pressure forces inside the volume and at the boundary, and the fourth integral is the dissipation due to surface and internal friction.

Palmén (1960) has shown that equation (13) can be transformed into the following form, which is more convenient for computational purposes:

$$\frac{A}{g}\frac{\partial}{\partial t}\int^{p} K\delta p=-\frac{L}{g}\int_{p_h}^{p_0}\overbrace{\hat{K}\hat{V}_n}^{\text{I}}dp+\frac{A}{g}\left[K\omega\right]_{p_h}$$

$$-\frac{L}{g}\int_{p_h}^{p_0}(\hat{\phi}-\bar{\phi})\,\overline{V}_n dp-\frac{L}{g}\int_{p_h}^{p_0}\overbrace{\phi''V''}^{\text{II}}dp$$

$$+\frac{A}{g}\left[\overline{\phi'\omega'}\right]_{p_h}-\frac{A}{g}\int_{p_h}^{p_0}\overbrace{\overline{\alpha'\omega'}}^{\text{III}}dp-\overbrace{\overline{A\rho c_p V_0^3}}^{\text{IV}}$$

$$-A\int_0^h\rho K_h\left[\left(\frac{\partial u}{\partial z}\right)^2+\left(\frac{\partial v}{\partial z}\right)^2\right]dz \quad (14)$$

where the first term on the right (term I in table 1) is the lateral transport of kinetic energy, the fourth term on the right (term II in table 2) is the work done on the boundary by asymmetries in the wind and geopotential fields, the sixth term on the right (term III in table 2) is the internal conversion of potential to kinetic energy, and the seventh term on the right (term IV in table 2) is the dissipation caused by surface friction. Other terms on the right include the vertical transport of kinetic energy through the top of the volume (second term), the work done by the mean pressure forces acting on the boundary (third term), the transport of potential energy through the top of the volume (fifth term), and the dissipation resulting from internal friction (last term). Following the convention of Palmén and Holopainen (1962), a bar operator denotes areal mean, a primed quantity denotes the deviation from the areal mean, a circumflex denotes a mean along the boundary, and the double prime denotes the deviations from the mean along the boundary. The two terms evaluated at p_h vanish because omega was assumed to be zero at the top of the volume (100 mb). The mean boundary work term was also vanishingly small due to the geostrophic assumption in evaluating the geopotential along the boundary. No attempt was made to evaluate the internal friction in equation (14). This will certainly be negative and possibly about the same order of magnitude as the surface friction term.

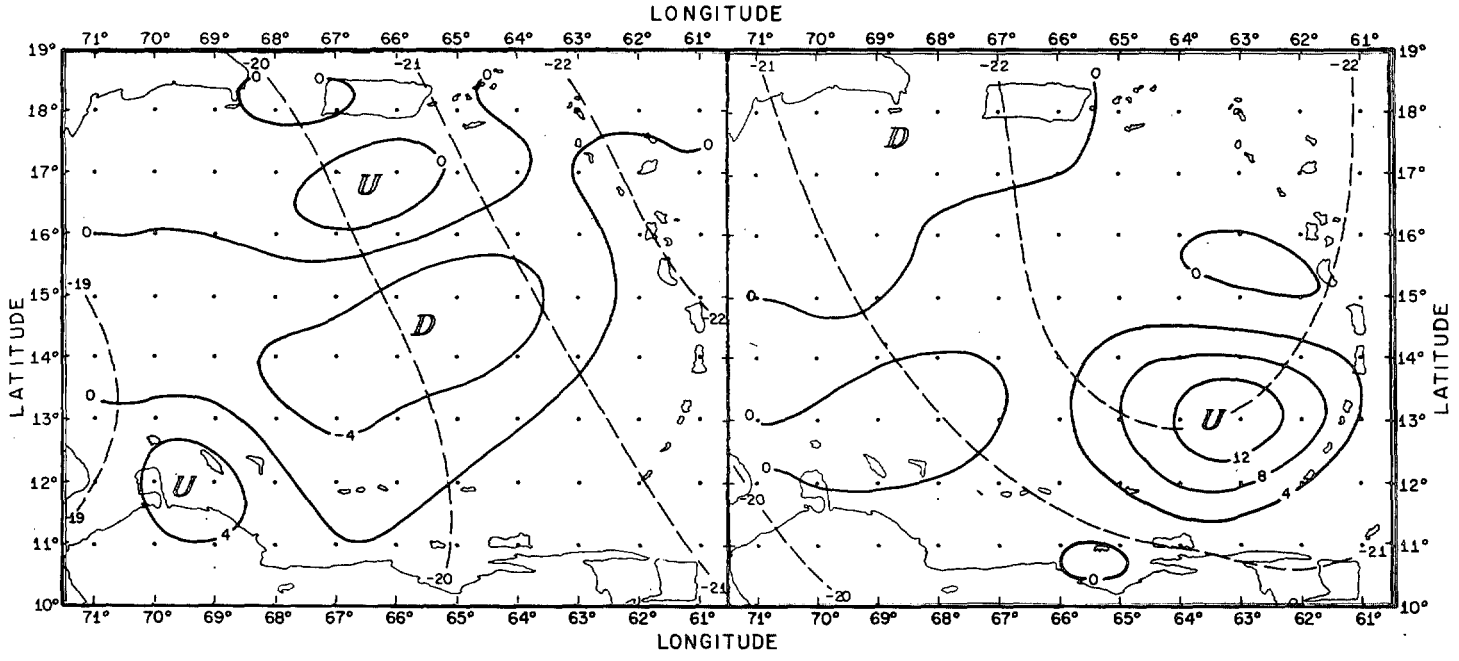

FIGURE 9.—Vertical motions at 400-mb (13th and 17th) computed by method A.

TABLE 2.—*Kinetic energy budget for the eastern Caribbean during Oct. 12–14 and 16–18, 1965*

		12	13	14	16	17	18	Composite
I	Advection of K.E.	+3.35	+3.62	+3.22	+0.92	+0.68	−0.06	+0.40
II	Eddy boundary work	−0.76	−0.41	+0.56	−0.69	−0.04	− .60	−2.59
	Mean boundary work							
III	$-\overline{\alpha'\omega'}$	+0.03	+0.09	+0.14	−0.11	−0.13	−0.03	−0.48
IV	Surface friction	−0.26	−0.45	−0.35	− .47	− .35	− .27	−1.05
	Total* (I+II+III+IV)	+2.36	+2.84	+3.54	− .35	+0.16	− .96	−3.70
V	$-\mathbf{V}\cdot\nabla\phi$	−0.99	−1.19	+1.05	−1.23	−0.24	−1.09	−3.61
	Total* (I+IV+V)	+2.10	+1.99	+3.92	−0.78	+0.08	−1.42	−4.26
	Total K.E. in volume†	+3.98	+4.89	+5.20	+3.40	+3.08	+1.95	

*In units of 10^{19} ergs sec^{-1}
†In units of 10^{24} ergs

Since it was not possible to calculate omega on the boundary and since the procedure used in calculating the boundary heights (that is setting the normal component equal to zero) greatly reduces the amount of work done on the boundary, the outer rows were eliminated from the boundary calculations, leaving an array of 17×21 points for the daily analyses and a 13×27 grid array for the composite. The results of these calculations are shown in table 2.

The total kinetic energy tendency was computed in two ways. The first total is the sum of advection, boundary work, internal conversion, and surface friction (terms I+II+III+IV), while the second total combines the boundary work and the internal conversion (terms II+III) into the production term $-\mathbf{V}\cdot\nabla\phi$ (term V), and is therefore the sum of terms (I+IV+V). The agreement is quite good; better agreement could probably be expected if the boundary work term had not been underestimated.

During the first 3 days, the kinetic energy inside the volume increased. The calculations show that this increase was caused largely by the lateral advection of energy into the volume from the environment. The eddy boundary was negative on the first 2 days, the volume doing work on the environment, but became positive on the third day. The internal conversion of potential to kinetic energy was positive but not large. During the last 3 days, the total kinetic energy within the volume decreased. The tendency calculations show a decrease on the 16th and 18th, while on the 17th the tendency indicates a nearly steady state. The lateral transport of kinetic energy was much smaller during the last 3 days than it was during the first half of the period. Negative transport on the 18th signifies an export of kinetic energy from the volume. The internal conversion term was still small on the last 3 days but was negative, signifying an indirect circulation within the volume.

When the kinetic energy tendency totals were averaged over the first 3 days, the mean tendency was found to be in the right sense, but was a little larger than the observed 48-hr increase in kinetic energy within the volume. Similarly, the tendency averaged over the last 3 days was in the right sense, but a slight underestimate of the observed decrease in kinetic energy. Even closer agreement between observed and calculated energy tendencies would be expected had not internal friction been neglected. In the composite case, the computed tendency shows that the cold Low was decreasing in intensity, all terms being negative except the lateral advection term which was slightly positive. The internal conversion term was much larger, and the advection term generally

TABLE 3.—*Energy conversion term* $\overline{(\alpha'\omega')}$ *evaluated over 150-mb levels for Oct. 12–14 and 16–18, 1965 (units, ergs gm^{-1} sec^{-1} × 10^{-1})*

Pressure (mb)	12	13	14	16	17	18	Composite case
925	0.022	0.148	0.272	0.175	0.044	0.010	0.696
775	.067	.119	.130	−0.034	−0.124	.035	
625	.047	.147	.249	− .353	− .256	−0.041	−0.829
475	.105	.339	.558	− .740	− .707	− .207	−2.879
325	.111	.272	.364	− .324	− .501	− .100	−2.083
175	−0.045	−0.135	−0.176	+0.136	+0.203	+0.030	+0.339
Summary	0.307	0.890	1.397	−1.140	−1.341	−0.273	−4.75

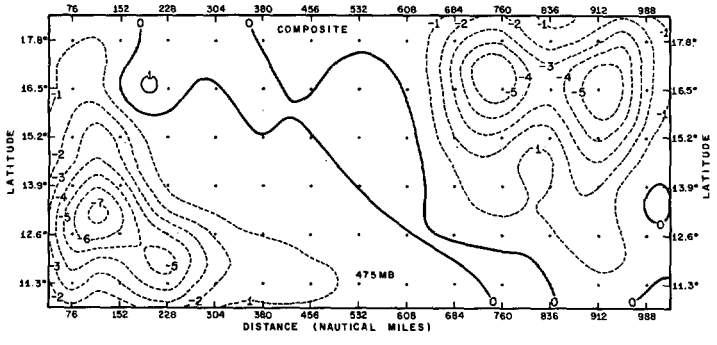

FIGURE 10.—Kinetic energy conversion term $(-\overline{\alpha'\omega'})$ at 475mb (that is the 400- to 550-mb layer) for the composite case, showing widespread conversion of kinetic to potential energy; limits are in ergs gm^{-1} sec^{-1}.

smaller that those of the individual days as the result of the larger volume considered.

While the area for the composite case does not contain the entire circulation of the cold Low, the calculations reflect a real decrease in intensity which occurred after the 13th or 14th of October. On these 2 days, winds in excess of 60 kt were observed at 250 mb (fig. 3), and the lowest level of closed circulation was near 850 mb. By the 17th, maximum wind speed observed at this level was little more than half that of the 13th, and the lowest level of closed circulation had risen to near 550 mb. A slow but progressive weakening of the temperature and geopotential gradients was also noted during this interval. On the 18th, the convective closed pattern appeared to be breaking up and becoming disorganized.

In table 3, the integrated values of $\overline{\alpha'\omega'}$ (by 150-mb layers) show that this term was uniformly positive in all but the top layer on the first 3 days and negative on the last 3 days at all levels but the top and bottom. Largest values are found in the upper troposphere. Also, figure 10 reveals the uniformly indirect nature of the composite circulation at a level (475 mb) where the greatest transformation from kinetic to potential energy was taking place. The dipolar pattern reflects cold air rising on the east and warm air descending on the west. Although the cold Low may have been operating in the direct sense on the first 2 or 3 days of the period, the composite results

TABLE 4.—*Kinetic energy budget for the eastern Caribbean during Oct. 12–14 and 16–18, 1965*

		12	13	14	16	17	18
I	Advection of K.E.		+3.81			+0.70	
II	Eddy boundary work		−0.55			+ .14	
	Mean boundary work						
III	$-\overline{\alpha'\omega'}$		+0.03			− 0.04	
IV	Surface friction		− 0.48			− .31	
	Total* (I+II+III+IV)		+2.81			+0.50	
V	$-\mathbf{V}\cdot\nabla\phi$		−1.20			−0.12	
	Total* (I+IV+V)		+2.13			+0.27	
	Total K.E. in volume†	+3.98	+4.98	+5.20	+3.40	+3.08	+1.95

*In units of 10^{19} ergs sec^{-1} † In units of 10^{24} ergs

show the net behavior of the system to be indirect over the 6-day period. Moreover, had the analyses encompassed the entire circulation of the cold Low, the results would likely have shown a still larger energy transformation and possibly a smaller boundary effect.

Finally, it should be stated that the energy calculations based upon the vertical motions obtained from the omega equation with either $\partial q/\partial t$ or the total heating H set to zero differed only slightly from those presented in table 1. In regard to the energy conversion term, $\overline{\alpha'\omega'}$, its magnitude decreased by about one-half, with neglect of $\partial q/\partial t$ and slightly more than that with $H=0$, its sign remaining unchanged.

The kinetic energy for the 13th and 17th, based on the vertical motions computed by method A, is listed in table 4. The results are almost identical to those in table 2 for the 13th, and the differences are not large on the 17th.

7. SUMMARY AND CONCLUSIONS

An upper tropospheric cold Low passed through the eastern Caribbean during a 6-day period in October 1965, when the area was the subject of intensive aircraft reconnaissance at several levels. Analyses based on the data collected by coordinated aircraft missions and special radiosonde ascents at island stations have been used to compute vertical motions and an energy budget for the region. In general, the agreement between computed vertical motions and weather was quite good for the 6-day composite case, but was slightly less satisfactory for the individual days. The computed kinetic energy tendencies were found to agree with the changes observed to take place within the volume. Conversion between potential and kinetic energy was small; most of the changes in kinetic energy in the domain were caused by boundary work plus lateral advection. During the 6-day period, the circulation within the volume changed from weakly direct to weakly indirect, although the results for the composite data show that the mean circulation was definitely indirect.

The overall satisfactory agreement between the computed results and observation would seem to indicate that the dynamical model employed is reasonably adequate

in its simulation of the tropical atmosphere. Conversely, this would suggest that the data themselves are suitable for numerical work.

REFERENCES

Carlson, Toby N., "Project ECCRO: A Synoptic Experiment in the Tropics," *ESSA Technical Memorandum* IERTM-NHRL 80, U.S. Department of Commerce, National Hurricane Research Laboratory, Miami, Fla., Aug. **1967***a*, 31 pp.

Carlson, Toby N., "Structure of a Steady-State Cold Low," *Monthly Weather Review*, Vol. 95, No. 11, Nov. **1967***b*, pp. 763–777.

Cressman, George P., "A Three-Level Model Suitable for Daily Numerical Forecasting," *Technical Memorandum* No. 22, U.S. Weather Bureau, Washington, D.C., **1963**, 22 pp.

Frank, Neil L., "The Weather Distribution With Upper Tropospheric Cold Lows in the Tropics," *Technical Memorandum* No. 28, U.S. Department of Commerce, Weather Bureau Southern Region, Ft. Worth, Tex., Oct. **1966**, 22 pp.

Kuo, H. L., "On Formation and Intensification of Tropical Cyclones Through Latent Heat Release by Cumulus Convection," *Journal of the Atmospheric Sciences*, Vol. 22, No. 1, Jan. **1965**, pp. 40–63.

Miller, Banner I., "Experiment in Forecasting Hurricane Development With Real Data," *ESSA Technical Memorandum* IERTM-NHRL 85, U.S. Department of Commerce, National Hurricane Research Laboratory, Miami, Fla., Apr. **1969**, 28 pp.

Palmén, Erik, "On the Maintenance of Kinetic Energy in the Atmosphere," *The Atmosphere and the Sea in Motion*, The Rockefeller Institute Press, New York, **1959**, pp. 212–224.

Palmén, Erik, "On the Generation and Frictional Dissipation of Kinetic Energy in the Atmosphere," *Commentationes Physico-Mathematicae*, Vol. 24, No. 11, Finska Vetenskaps-Societeten, Helsinki, **1960**, 15 pp.

Palmén, Erik, and Holopainen, E. O., "Divergence, Vertical Velocity and Conversion Between Potential and Kinetic Energy in an Extratropical Disturbance," *Geophysica*, Vol. 8, No. 2, **1962**, pp. 89–112.

Ricks, R. L., "On the Structure and Maintenance of High Tropospheric Cold-Core Cyclones of the Tropics," unpublished M.S. thesis, Department of Meteorology, University of Chicago, **1959**, 32 pp.

Sanders, Frederick, and Burpee, Robert W., "Experiments in Barotropic Hurricane Track Forecasting," *Journal of Applied Meteorology*, Vol. 7, No. 3, June **1968** pp. 313–323.

[*Received October 13, 1969; revised January 9, 1970*]